ACS Sustainable Chemistry & Engineering

Research Article

Cite This: ACS Sustainable Chem. Eng. 2019, 7, 4801−4813

pubs.acs.org/journal/ascecg

Highly Efficient and Durable Piezoelectric Nanogenerator and Photo-power cell Based on CTAB Modified Montmorillonite Incorporated PVDF Film

Prosenjit Biswas,[†] Nur Amin Hoque,[†] Pradip Thakur,[*,‡] Md. Minarul Saikh,[†,§] Swagata Roy,[†] Farha Khatun,[†] Biswajoy Bagchi,[∥] and Sukhen Das[*,†]

[†]Department of Physics, Jadavpur University, 188 Raja S. C. Mullik Road, Kolkata 700032, India

[‡]Department of Physics, Netaji Nagar College for Women, 170/13/1 N. S. C. Bose Road, Regent Estate, Kolkata 700092, India

[§]Government General Degree College at Pedong, Sakiyong Khasmahal, West Bengal 734311, India

[∥]Department of Medical Physics and Biomedical Engineering, University College London, Gower Street, Bloomsbury, London WC1E 6BT, United Kingdom

Supporting Information

ABSTRACT: Herein, we have successfully designed two ecofriendly, biocompatible, and cost-effective devices, i.e., a piezoelectric nanogenerator (PENG) and a self-charged photo-power cell (PPC) by developing a multifunctional cetyltrimethylammonium bromide (CTAB) modified montmorillonite (MMT) incorporated poly(vinylidene fluoride) (PVDF) thin film with large electroactive β crystallites and dielectric properties. Incorporation of CTAB modified MMT in PVDF leads to nucleation of piezoelectric β crystallite ($F(\beta)$) ~ 91% as well as the dielectric constant ~48 at 3 mass % doping of CTAB-MMT. The enrichment of the electroactive β phase crystallization and high dielectric constant pilot to a good piezoelectricity (d_{33}) ~ 62.5 pC/N at 50 Hz of the thin film. Our CTAB-MMT/PVDF based PENG (CMPENG) with superior piezoelectricity shows high output power generation with power density ~ 50.72 mW/cm^3 under periodic finger impartation and having the ability to charge a 1 μF capacitor up to 2.4 V within 14 s under gentle finger impartation. CMPENG also have the potential to glow up commercially available 26 blue light-emitting diodes (LEDs) connected in series. The self-charged PPC has been designed with the thin film in association with MnO_2-MWNT/PVP/H_3PO_4. Our PPC is able to generate supercilious output voltage ~ 1.38 V and short circuit current ~ 3.7 mA/cm^{2}under light illumination with specific areal capacitance and energy storage efficiency of ~1501 F/m^2 and ~93%, respectively. The realistic application of our PPC is investigated by lighting 24 blue LEDs for 7 days with the same intensity by charging the device once for 50 s.

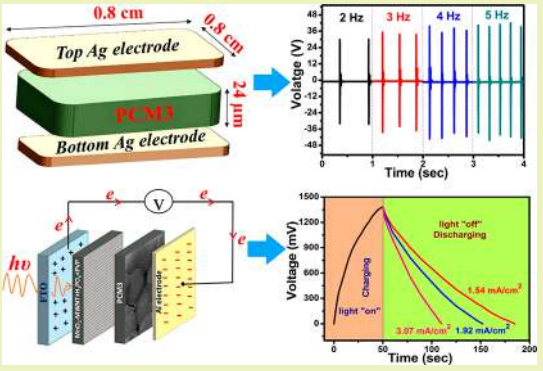

KEYWORDS: *MMT, PVDF, Dielectric, Piezoelectric, Energy, Power density*

INTRODUCTION

Increase of energy expenditure of our modern societies and the depletion of traditional fossil fuels such as coal, petroleum, and so on have polarized the scientific community with deep concern about the development of novel energy harvesting materials as well as simple techniques to design highly efficient energy generating and storage devices to exploit sustainable and green energy for miniaturization and multifunctionalization in electronics industry. Our daily life is being surrounded by various types of multifunctional modish electronic gadgets such as mobile phones, tablets, laptops, and sensors, etc., which are driven by conventional electrochemical or lithium ion batteries for a long time period.[1−4]

Now it is the time to minimize use of power consumption from traditional resources of energy, which are associated with environmental pollutions and global warming issues.[1−4] Recently, energy harvesting from our living systems such as mechanical energy linked with human movement, air flow, and sea waves, etc., and solar energy along with storage in the same unit are highly appreciated by scientists and engineers due to its environmentally friendly nature and cost-effectiveness.[4−12] Energy harvesting and its storage have two different issues. Designing of a portable hybrid device by integrating an energy conversion and storage part in a single unit with superior performances is not only very promising but also very challenging.[4,5,12] Though few such types of hybrid systems have been reported previously, development of highly efficient

Received: October 3, 2018
Revised: January 30, 2019
Published: February 12, 2019

DOI: 10.1021/acssuschemeng.8b05080
ACS Sustainable Chem. Eng. 2019, 7, 4801−4813

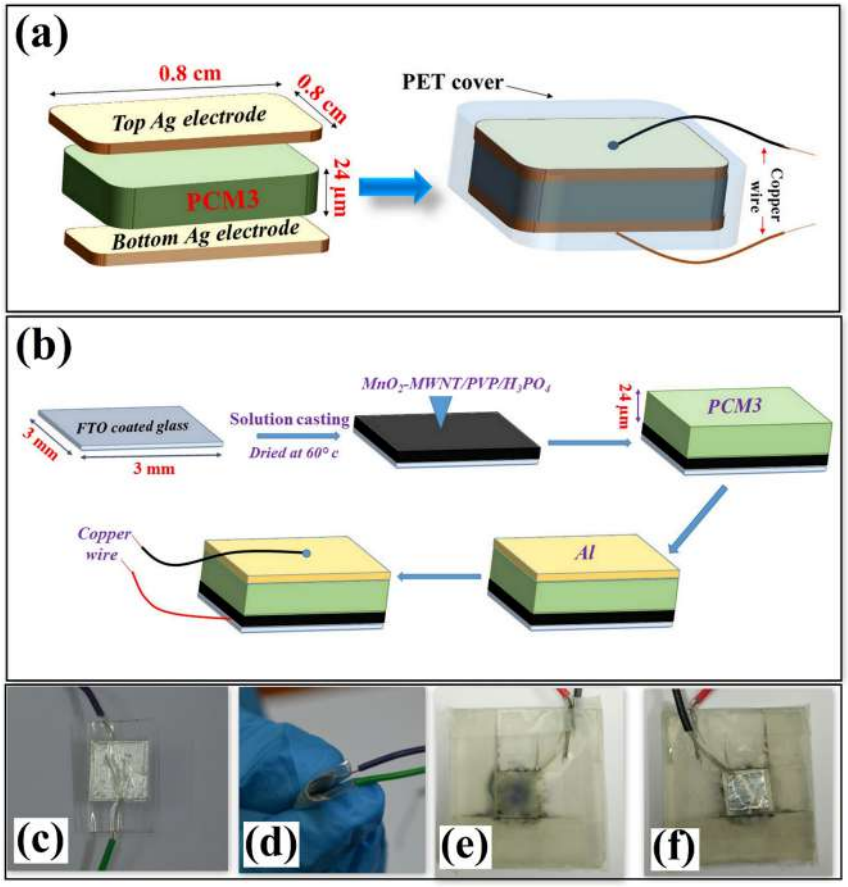

Figure 1. Schematic diagram of the fabricated (a) CMPENG and (b) self-chargedPPC. (c, d) Digital images and photography of the flexibility test of CMPENG. (e, f) Digital photographs of PPC for both side.

integrated devices is still far away for direct practical utilization in our daily portable gadgets.[5,8,12,13]

Scientists have developed a promising energy harvesting technique for converting direct mechanical energy to electrical energy via piezoelectric response by piezoelectric nanogenerators (PENGs).[14−16] Traditional piezoelectric materials or ceramics such as PZT, $ZnSnO_3$, PMN−PT, $BaTiO_3$, ZnO, and (Na,K)-NbO_3 have been studied widely for developing the PENGs. There are some limitations of those types of materials for versatile utilization due to their high weight and nonflexibility.[4,15−19] Recently, electroactive poly(vinylidene fluoride) (PVDF) and its copolymers have emerged as a most promising material for designing flexible, lightweight, cost-effective, and environmentally friendly PENGs.[4,14,20]

Also high dielectric PVDF and PVDF based nanocomposites (NCs) have the ability to store electrical energy.[4,12] A PVDF based sophisticated self-charged power cell might be designed by proper techniques and choosing genuine materials. A self-charged photo-power cell is a new concept of such a self-charged power cell for portable energy demands of electronic applications.[4,5,12] Integration of solar cells, i.e., photovoltaic cells along with a supercapacitor or lithium ion cells, are carried out by some scientists and engineers.[21−28] The overall performances and storage ability of such hybrid cells are converged as the integration between the energy harvester part and the storage part is carried out through external circuits which enhanced the overall resistances and sunlight illumination. These shortcomings may be overcome by proper design of a two electrode self-charged photo-power system where energy creation and storage occur in same unit. A photo-supercapacitor was previously reported by Wee et al., where an organic photovoltaic (OPV) was integrated with carbon nanotube (CNT) in one unit.[21] PVDF based photovoltaic cells with energy storage function also reported by Zhang et al. (energy density (E) = 1.4 mWh kg^{-1}).[29]

PVDF is a semicrystalline electroactive plastic polymers having five different polymorphs, α, β, γ, δ, and ε, on the basis of bond orientation of -CH_2 and -CF_2 dipoles. Here, the thermodynamically highly stable nature of the nonpolar α crystalline phase (TGTG′ dihedral conformation) directly formed through the melting process. The γ-phase having TTTGTTTG′ conformation gives average piezoelectricity due to its polar nature. Among the polar β, γ, and δ forms of PVDF, the all-trans (TTTT) conformation of the polar β-crystalline phase results in optimum maximum piezoelectric, pyroelectric, ferroelectric, and dielectric properties with promising elastic strength.[4,30,31]

Thus, a simple, low cost technique is required to improve the electroactive β-phase formation as well as the dielectric properties of PVDF for applying in the field of energy harvesting unit and energy storage systems. The traditional procedure to nucleate β-polymorph in PVDF is "poling" by the external electric field and mechanical stretching on α-PVDF.[32,33]Apart from these processes self-poled electroactive β-PVDF has also been achieved via impregnation of the polymer matrix with different kinds of nano-/microfillers such as metal nanoparticles (NPs),[34] metal oxide NPs,[35−37] ceramic NPs,[38] metal salts,[14,39−41] carbon nanotube,[42] organic

DOI: 10.1021/acssuschemeng.8b05080
ACS Sustainable Chem. Eng. 2019, 7, 4801−4813

molecule,[5,12] and clays,[43−47] etc. Proper choice of fillers and their homogeneous incorporation into PVDF not only improve the nucleation of β-crystals but also enhance the dielectric properties due to enhancement of electric dipoles via large interfacial polarization. Developed high dielectric and electroactive β-phase enriched PVDF have the potential to design optimized PENGs as well as multifunctional hybrid devices such as a photopower bank which is able to harvest and reserve the electrical energy in the same unit. Though numerous studies on MMT doped PVDF composites were carried out regarding their electroactive phase nucleation behavior in PVDF, dielectric, filtration, and thermal properties.[44−47] Nevertheless, no such study henceforth has been carried out using cetyltrimethylammonium bromide (CTAB) modified MMT as a dopant assisting in the β-phase crystallization as well as improvement of dielectric properties of PVDF. Here CTAB has been used to modify the MMT surface so that we can achieve well and homogeneous dispersion of CTAB-MMT in PVDF matrix to ensure intimate interaction and binding between the PVDF chains and MMT sheets through CTAB molecules. Intimate interaction and binding between the CTAB-MMT and PVDF chains lead to alignment of the polymer chains in all-trans conformation (TTTT), i.e., nucleation of the electroactive β phase as well as the dielectric property through interfacial polarization effect.

Thus, we have successfully developed electroactive β-crystallite prosperous and improved dielectric PVDF composite films via incorporation of CTAB-MMT via simple solution casting procedure. Thereafter, a prototype PENG (named as CMPENG) and a self-charged photo-power cell (named as PPC) have been demonstrated using the optimized CTAB-MMT/PVDF film for energy harvesting and storage, respectively. MnO_2-MWCNT/PVP/H_3PO_4 composite thin film has been used as the light absorbing and electron generation part in the PPC. The devices show excellent output characteristics and durability over a long period with promising practical application possibilities in portable and large scale areas of electronic gadgets.

EXPERIMENTAL SECTION

Synthesis of PCM Composite Thin Films. CTAB-MMT(CM)/PVDF composite thin films are prepared via simple solution casting method. Herein 5 mass % PVDF (Aldrich, Germany; M_w = 275000 GPC; M_n = 110 000) solution (prepared by mixing 250 mg of PVDF in 5 mL of dimethyl sulfoxide (DMSO; Merck India) stirred at 60 °C for 2 h) was added with CTAB-MMT (1, 2, 3, 4, and 5 mass %). Then the mixture was vigorously stirred for 6 h at 60 °C followed by ultrasonication (30 min) for obtaining homogeneous mixture. Then the mixture was casted in clean Petri dishes and dried at 80 °C for 12 h to obtain composite films by complete vaporization of DMSO. Pure PVDF thin film was also prepared keeping the same condition without mixing any dopant. Finally we obtained the composite films named as PCM1, PCM2, PCM3, PCM4, and PCM5, which contained 1, 2, 3, 4, and 5 mass % CM content in PVDF matrix, respectively.

CMPENG Fabrication. The CMPENG was designed with PCM3 thin film with dimensions ~0.8 cm × 0.8 cm × 24 μm. Silver electrodes of thickness 6 μm were pasted on both surfaces of the film, and Cu wires were extended out from both electrodes. Finally, the whole system was sealed with poly(ethylene terephthalate) (PET), keeping outside the end of the two Cu wires for measuring the output characteristics of our designed CMPENG (Figure 1a,d).

PPC Fabrication. Initially, 50 mg of MnO_2-MWCNT (see Supporting Information for detailed preparation process) and 500 μL of *o*-phosphoric acid (H_3PO_4; Merck India) were added to previously prepared 10% poly(vinylpyrrolidone) (PVP; Loba Chemie) solution in water. Then the entire mixture was stirred for 1 h at room temperature to obtain a homogeneous mixture. This mixture has been deposited on FTO coated glass and dried at 60 °C until a sticky layer has been obtained. Then the counter electrode (Al foil) of dimensions ~ (0.3 cm × 0.3 cm × 24 μm) containing pure PVDF or PCM3 thin film was introduced on the sticky layer and dried at 60 °C for 30 min for proper adjoining and complete vaporization of water. Two copper wires were connected to two terminals of the device; i.e.. one was connected with FTO and another with aluminum foil to check the performances of our self-charged PPC (Figure 1e,f).

Characterization Technique. The surface morphology and microstructures of the sheet type MMT into the polymer matrix were observed by a field emission scanning electron microscope (FESEM; INSPECT F50, The Netherlands).

The nucleations of the electroactive β phase in the samples were investigated using an X-ray diffractometer (Model-D8, Bruker AXS Inc., Madison, WI, USA) at room temperature with operating voltage of 35 kV and current 35 mA with a scan speed of 0.3 s/step and with 2θ range from 15° to 35° using Cu Kα radiation.

Then the effects of CM on β-phase nucleation in the samples were further characterized using Fourier transform infrared spectroscopy (FTIR 8400S, Shimadzu). Here to obtain the absorbance of IR spectroscopy, the wavenumber range was set from 400 to 1100 cm^{-1}, keeping resolution at 4 cm^{-1} and scanning each sample for 50 times. From the IR spectra of each sample the fraction of β-phase content ($F(\beta)$) was calculated following the Lambert−Beer law:

$$F(\beta) = \frac{A_\beta}{\left(\frac{K_\beta}{K_\alpha}\right)A_\alpha + A_\beta} \quad (1)$$

where A_β and A_α are the absorbances at 840 and 764 cm^{-1}, respectively, and K_β (7.7×10^4 cm^2 mol^{-1}) and K_α (6.1×10^4 cm^2 mol^{-1}) represent the absorption coefficients of those wavenumbers, respectively.[12,14]

The dielectric behavior of the samples was studied using a digital LCR meter (Agilent, E4980A) for the frequency range from 20 Hz to 2 MHz and applying 1 V signal between two surfaces of the sample using a sample holder containing circular Ag electrodes under ambient conditions. Using eqs 2 and 3, the dielectric constant (k) and ac conductivity (σ_{ac}) were estimated respectively,

$$k = Cd/\varepsilon_0 A \quad (2)$$

$$\sigma_{ac} = \omega\varepsilon_0 k \tan\delta \quad (3)$$

Here, C, d, A, ε_0, and ω represent the capacitance, thickness, area of the samples, free space permittivity, and angular frequency applied between two surfaces of the films, respectively.[4]

The output characteristics of our PPC were investigated with the help of a digital multimeter (Agilent U1252A) and an electrometer (Keysight- B2985A). The performance of CMPENG is measured by a digital storage oscilloscope (Keysight, Oscilloscope DSO-X 3012A).

RESULTS AND DISCUSSION

The multifunctional PCM film has been utilized successfully to design two devices CMPENG and self-charged PPC (fabrication process detailed in CMPENG Fabrication and PPC Fabrication, respectively). Schematic diagrams of the two device are demonstrated in Figure 1a,b, respectively.

Here we utilize CM loaded PVDF composite (PCM) film for realistic multifunctional applications. First, we have optimized the multifunctional CM assisted electroactive and high dielectric PVDF film via proper characterization and choose the best prospectus for designing the devices. CM loaded PVDF thin film is the origin of piezoelectricity of the nanogenerator which responds under touching and converts mechanical energy into electrical energy. In a photovoltaic self-

DOI: 10.1021/acssuschemeng.8b05080
ACS Sustainable Chem. Eng. 2019, 7, 4801−4813

charging power bank, the high dielectric and electroactive PCM thin film acts as a storage part.

Characterization for Device of CM Modified PVDF Thin Films. *Surface Morphology and Microstructure Analysis.* Figure 2 represents the microstructure and surface morphology of pure PVDF and CM modified PVDF thin films. Uniform distribution and strong interaction of the MMT sheets into the polymer matrix can be described in the FESEM images (Figure 2b–f). Panels g–l of Figure 2 represent the different morphological changes, i.e., formation of domains in the pure PVDF and CM doped PVDF films (see the Supporting Information). FESEM image of pure PVDF shows formation of domains with diameter ∼ 50–60 μm (Figure 2g), whereas for PCM1, PCM2 and PCM3 samples formation of smoothened uniform spherulites with smaller diameter ∼ 5 μm are clearly observed (Figure 2h–j). The formation of small spherical domains with clear boundary and enhanced smoothness is attributed to formation of electroactive β crystallites.[39] But for higher CM doping, i.e., PCM4 and PCM5 samples, the spherulites are not grown properly and the smoothness of the spherulites are decreased indicating reduction of β crystal nucleation in the samples (Figure 2k,l).[39]

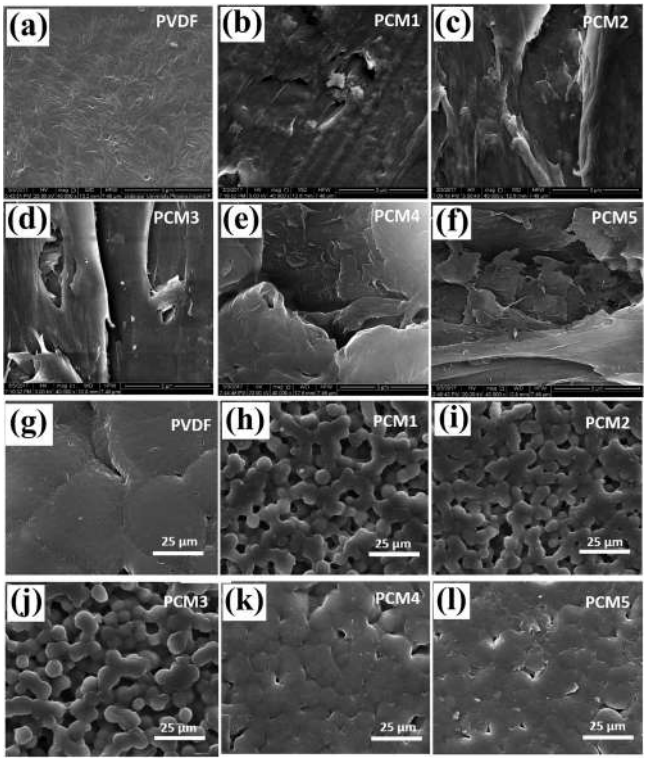

Figure 2. (a) FESEM micrograph of pure PVDF. (b–f) Surface morphology of the CM assisted PVDF composite thin film. (g–l) Formation spherulites in pure PVDF and the CM loaded PVDF samples.

X-ray Diffraction Analysis. Electroactive β-phase formation into the polymer matrix have been studied by the X-ray diffraction pattern. Figure 3a represents the XRD pattern of pure PVDF and CM modified PVDF films.

For pure PVDF, XRD patterns show peaks at 2θ = 17.6° (100), 18.3° (020), 19.9° (021), and 26.6° ((201), (310)),- which refer to the presence of nonpolar α-phase. After addition of CM into the polymer matrix, the characteristic peak of electroactive β-phase appear prominently at 20.6°((110), (200)) vanishing all peaks corresponding to α phase in composite samples. Also a small diffraction peak is observed at 36.8° ((020), (100)) for PCM3 and PCM4 sample which is also due to electroactive β-phase.[4,14,44] These indicate that the crystallization of β-phase is accelerated due to catalytic effect of CM. Closer investigation indicates that the intensity of main β-phase peak at 2θ = 20.6° increases with increasing mass % CM and maximized for 3 mass % loading of CM. A qualitative idea about the amount of β-phase and α-phase content may be obtained by calculating the ratio of the intensity $I_{20.6}$ and $I_{18.3}$ shown in Figure 3b. The ratio of the intensity $I_{20.6}$ and $I_{18.3}$ has been found for the PCM3 film indicating formation of maximum β phase at that concentration.

Fourier Transform Infrared Spectroscopy. Electroactive β-phase nucleation in the PCM samples have further been confirmed by the FTIR spectroscopy shown in Figure 3c. The IR spectrum of pure PVDF represents absorbance peaks at 487 cm^{-1} (wagging of CF2 bond), 531 cm^{-1} (CF2 bonds bending), 616 and 764 cm^{-1} (CF2 skeletal bending), 796 and 976 cm^{-1} (CH2 rocking) indicating the presence of nonpolar α-crystallite. After incorporation of CM into the PVDF matrix, all the absorbance peaks associated with α-phase are diminished and the absorbance peaks appear at 479 cm^{-1} (CF_2 deformation), 510 cm^{-1} (CF_2 stretching), 600 cm^{-1} (CF_2 wagging), and 840 cm^{-1} (CF_2 stretching, CH_2 rocking, skeletal C–C) indicating the electroactive β-phase nucleation in PCM thin films.[4,12,45] With increasing the amount of CM into the polymer matrix, the intensity of the main β-phase peak at 840 cm^{-1} increases to PCM3 due to catalytic activity of the CM particles which is compatible with X-ray diffraction analysis. Further doping of CM in PVDF (i.e., PCM4 and PCM5) confines the free movement of the chains of the polymer and the nucleation of electroactive β polymorph in the PCM4 and PCM5 samples as the nucleation points increases so many that the β spherulites cannot be developed properly. Thus, β-phase nucleation is reduced at higher doping of the CM which is also confirmed by FESEM image shown in Supporting Information (Figure S6).

Furthermore, $F(\beta)$ in the samples has been calculated using eq 1. The histograms of F(β) with the varying mass content of CM into the PVDF matrix are shown in Figure 3d. The obtained maximum β phase content is∼ 91% for PCM3.

The formation of β-phase crystallization has been justified very clearly by FESEM, XRD, and FTIR data. The driving factor for β phase transformation in CM loaded PVDF matrix may be the outcome of well interaction between the − CH_2/ CF_2 dipoles of PVDF chains and charged surfaces of CM sheets resulting in longer polymer chain of *all-trans* conformation, i.e., TTTT configuration.[4,30]

Dielectric Behavior Analysis. The dielectric properties, i.e., dielectric constant, tangent loss, and conductivity of the pure PVDF and CM assisted PVDF composite films, have been investigated with varying the CM mass percent into the polymer matrix and frequency under the ambient condition. Panels a and b Figure 4 represent the frequency dependency of dielectric constant and tangent loss in the range from 20 Hz to 2 MHz. With increasing frequency, the dielectric constant and tangent loss have been decreased for all films. Confinement of the movement of the dipoles with increasing frequency reduces the net Maxwell–Wagner–Sillars (MWS) interfacial polarization as dielectric constant. At the lower frequency range the dipoles are able to follow the externally applied ac electric field, whereas the movements of the dipoles are restricted at the

DOI: 10.1021/acssuschemeng.8b05080
ACS Sustainable Chem. Eng. 2019, 7, 4801–4813

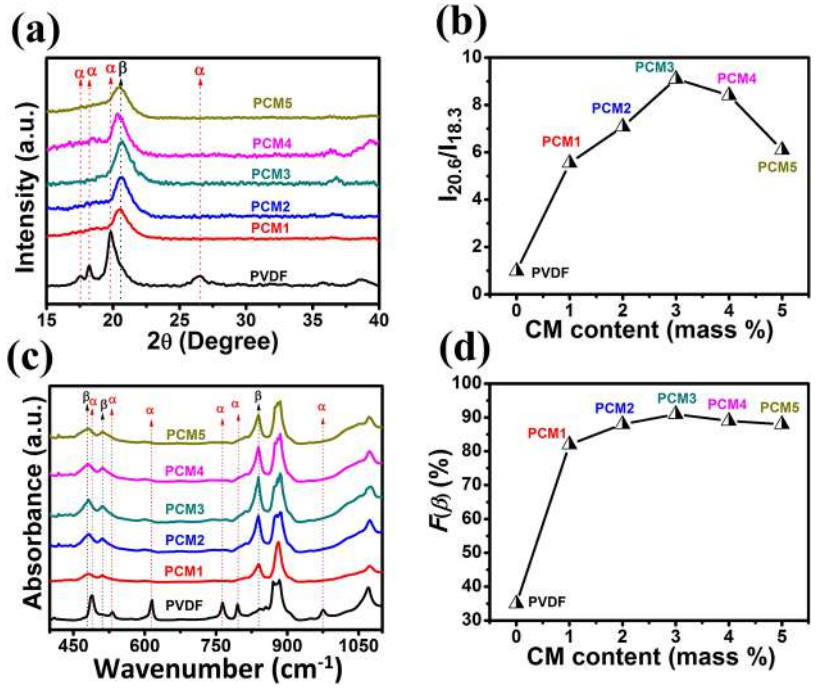

Figure 3. (a) XRD pattern of pure PVDF and PCM composite thin films (PCM1, PCM2, PCM3, PCM4, and PCM5). (C) Ratio of $I_{20.6}$ and $I_{18.3}$ of the samples measured from XRD spectra. (c) FTIR spectra of pure PVDF and CTAB-MMT/PDVF composite thin films. (d) β-phase content of the samples calculated from FTIR spectra.

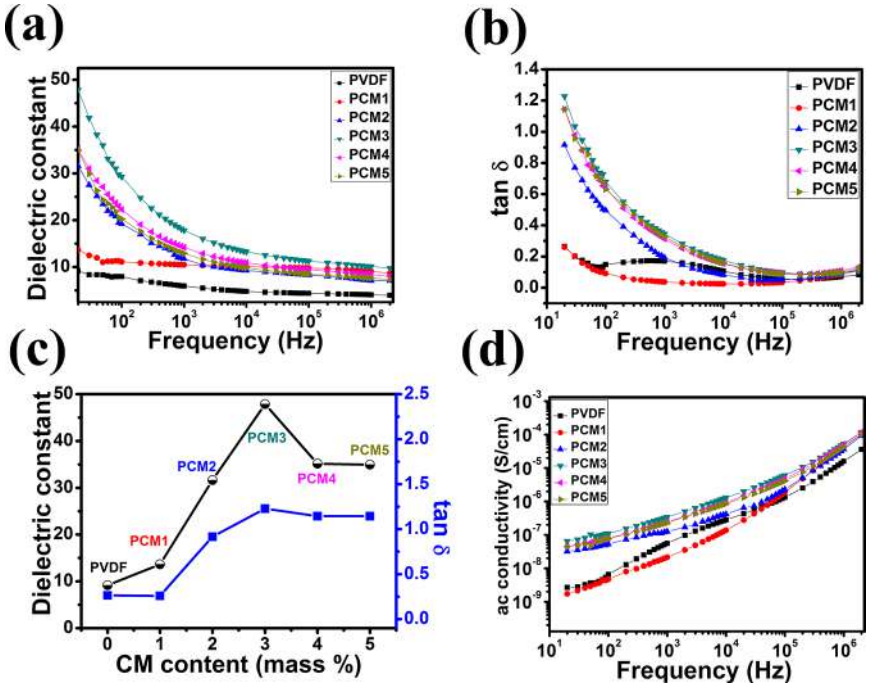

Figure 4. (a, b) Variation of dielectric constant and tangent loss of unblended PVDF and PCM thin films with frequency. (c) CTAB-MMT content dependent dielectric constant and tangent loss. (d) Frequency dependent ac conductivity of unblended PVDF and PCM thin films.

higher frequency region. Thus, the dipoles lag behind the electric field and lead to decrease in dielectric constant with increasing frequency.[4,14,48]

With increasing the doping concentration of CM into the polymer matrix, the dielectric value as well as tangent value also increases (Figure 4c). The maximum dielectric constant ~ 48 (where for unblended PVDF, the value of dielectric constant is just ~9) with very low tangent loss 1.22 has been obtained for 3 mass % doping of CM in PVDF at the frequency 20 Hz. Introduction of the CTAB-MMT in PVDF matrix leads to alignment of the polymer chains in all-trans conformation (TTTT), i.e., nucleation of electroactive β phase, and enhances the interfacial areas and the dipoles in the composite samples, which leads to improvement of dielectric property through interfacial polarization effect, i.e., MWS interfacial polarization effect. The charge accumulation at the interfaces between the

DOI: 10.1021/acssuschemeng.8b05080
ACS Sustainable Chem. Eng. 2019, 7, 4801−4813

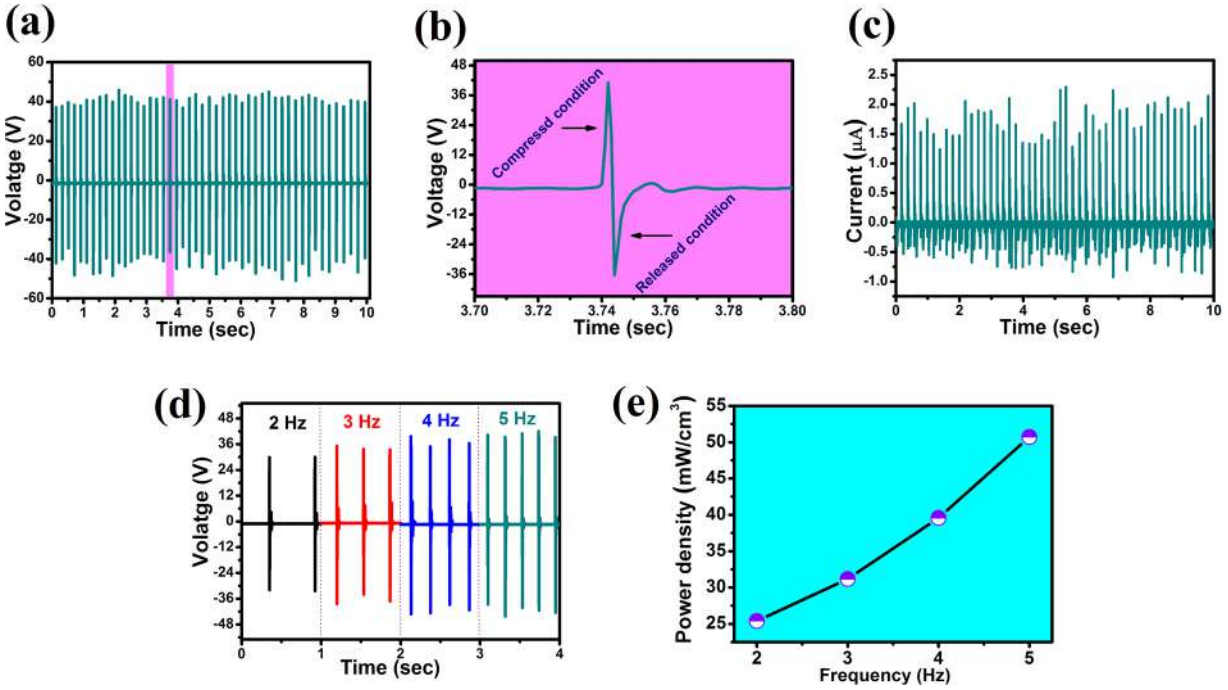

Figure 5. (a–c) Open circuit voltage (V_{oc}), magnified view of V_{oc}, and short circuit current (I_{sc}) of CMPENG under repetitive finger impartation. (d) Frequency dependent output voltage and power density of CMPENG under constant force.

CM sheets and PVDF matrix and formation of β-phase content through electrostatic interaction between the CM sheets and polymer chains have increased with increasing CM concentration and maximized at 3 mass % of CM doping in PVDF (Figure 2 and Figure 3). Consequently, the interfacial polarization via MWS effect has been maximized upon reaching the percolation threshold value of the dopant, i.e., at 3 mass % doping of CM in PVDF, which results maximum dielectric value (~48) in the PCM3 sample. Further loading of the CM sheets leads to agglomeration and decreases the interfacial surfaces between the CM sheets and the PVDF matrix as well as reduction in β-phase nucleation (Figure 2 and Figure 3). So, the dielectric value is reduced for higher concentration, i.e., for PCM4 and PCM5. Figure 4d demonstrates the variation of ac conductivity in the frequency range from 20 Hz to 2 MHz. ac conductivity increases with the increasing frequency due to MWS effect between the interface of CM sheets and polymer matrix.[4,14,43,47,48]

Thus, we have successfully achieved our optimized multifunctional sample named as PCM3 with highest electroactive β-phase content and dielectric value. The piezoelectric coefficient (d_{33}) value of PCM3 is measured to be ~62.5 pC/N at 50 Hz by Piezotest, PM300. This PCM3 thin film has been used for fabricating our two prototype devices.

Performances and Mechanism of CMPENG. Designing of CMPENG with the highest electroactive PCM3 film has been detailed in Experimental Section "CMPENG Fabrication". Under the application of periodic force via finger touching (force ~ 12 N), our prototype CMPENG generates excellent output characteristics, i.e., open circuit voltage (V_{oc}), the short circuit current (I_{sc}), and the superior power density shown in Figure 5. The CMPENG successfully produces superior power density ~ 50.72 mW/cm^3 with V_{oc} ~ 41 V and I_{sc} ~ 1.9 μA under finger impartation (~12 N) illustrated in Figure 5a,c, respectively. The frequency dependent output characteristics, i.e., V_{oc} and power densities, have been demonstrated under constant force and shown in Figure 5d,e, respectively. The output piezoelectric voltage becomes maximum at 5 Hz, which may be due to the enhancement of current with better impedance matching in the measured system. At higher imparting frequency the restoring of the CMPENG to its original state may be restricted and the impedance of the system might be mismatched, which lead to a decrease in output voltage.[4,49] To check the longevity, the output performances of our CMPENG are observed for 10 weeks (one cycle of 400 s per week). The output performance remains almost the same for a long period of 70 days. (See Figure S4 in the Supporting Information.)

To explore the superior performances and stability of our CMPENG in realistic utilization, the capability of the device is investigated by charging a capacitor and glowing up commercially available light-emitting diodes (LEDs). The superiority of our device is examined by charging a capacitor (1 μF) under repetitive finger touching, which is connected through a four probe bridge rectifier circuit shown in Figure 6a. Our CMPENG is capable of charging the capacitor up to ~2.4 V in 14 s under cyclic finger impartation. The typical charging pattern of the capacitor is similar to the exponential curve shown in Figure 6b. Instantaneous mechanical energy to electrical energy conversion efficiency (η) ~ 60.2% has been calculated in the capacitor charging process (see Table S1 of the Supporting Information for calculation). The comparative study of output characteristics and mechanical to electrical energy conversion efficiency of our CMPENG have been executed with previously reported PENGs and shown in Tables S2, S3, and S4 (see the Supporting Information). The comparative study implies the superiority of our CMPENG over other previously reported PENGs elsewhere. The ability of fast charging phenomenon of our talented device may be proposed for the direct application probabilities such as touch sensor, mobile charging under just finger touching. Our CMPENG is also able to light up 26 blue LEDs (connected in

DOI: 10.1021/acssuschemeng.8b05080
ACS Sustainable Chem. Eng. 2019, 7, 4801–4813

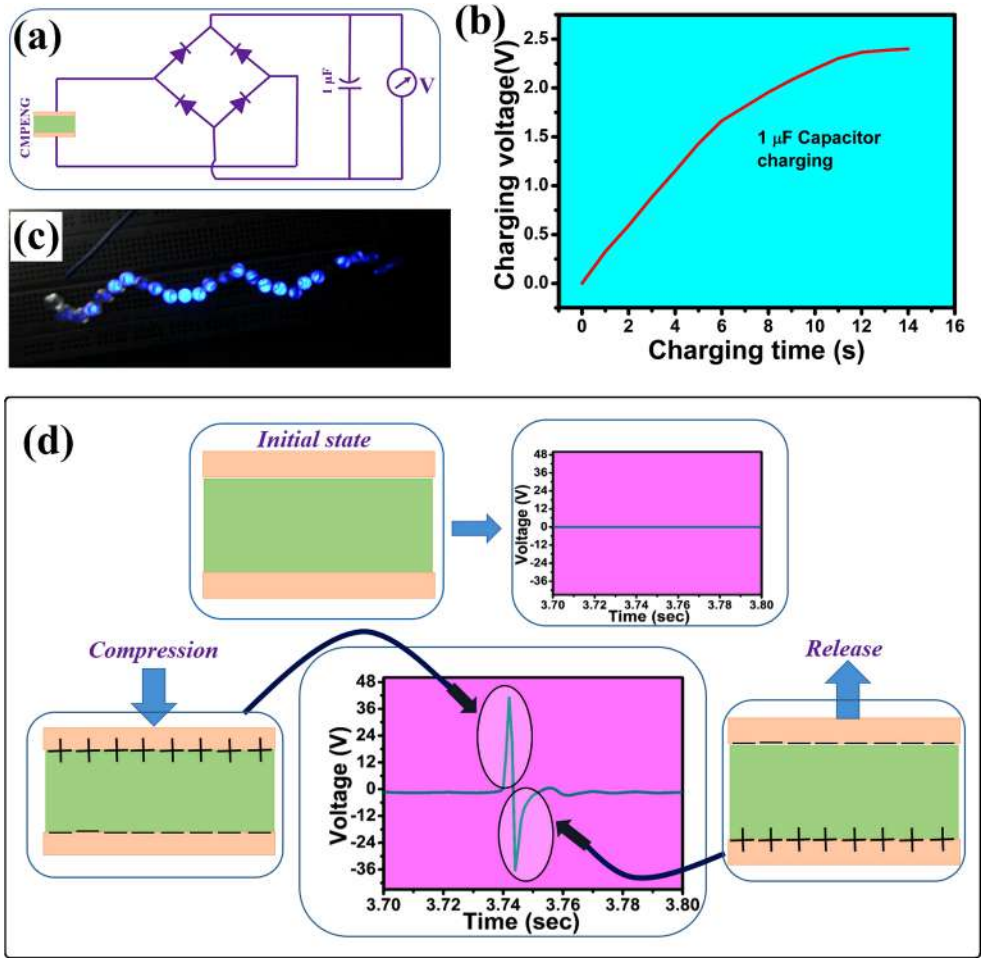

Figure 6. (a) Schematic diagram of capacitor charging circuit. (b) Capacitor charging (voltage vs time) graph by using CMPENG under repetitive finger impartation. (c) Snapshot of glowing blue LEDs driven by CMPENG. (d) Schematic representation of working mechanism of our CMPENG via piezoelectric effect under repetitive finger impartation.

series) under periodic finger impartation and relaxation (see Figure 6c and Video S1).

Further we have checked the piezoelectric output data in bending mode as well as connecting in reverse mode to clarify the triboelectric effect. The output data in bending mode are found to be very small, ~60 mV (peak to peak voltage), proving the negligible contribution to the obtained output data by triboelectric effect. The output characteristics in reverse connection mode are just similar to the piezoelectric data obtained in direct connection mode (Videos S3 and S4). Also the output voltage is well consistent with the piezoelectric coefficient value which is compared in the Supporting Information. Thus, the triboelectric contribution to piezoelectric output data is very negligible. Figure 6d illustrates the possible mechanism of generation of electrical energy under repetitive finger impartation and relaxation. The generation of electric voltage under mechanical force can be explained by the piezoelectric effect due to polar dipoles present in the PCM3 sample. The electrostatic interaction between the CM sheets and the -CH_2/CF_2dipoles of PVDF induces self-polarization and the alignment of polymer chains in all-trans configuration which leads to electroactive β phase formation in the polymer matrix. This self-polarization effect activates the piezoelectric voltage generation. The dipole movement through the crystal lattice as well as redistribution and displacement of the dipoles in the self-poled polymer matrix under external force by finger impartation lead to development piezoelectric voltage.[4,14,50] In addition, when an external force is applied, the alignment of dipoles into the crystal along the applied mechanical stress has also triggered induced polarization without any type of external bias field. The rising of self-polarization effect of piezoelectric material due to combination of induced surface charge polarization and stress drives the excellent output performance. When a vertical compression is applied on our CMPENG, the top electrode has acquired positive polarization charge and at the same time the same amount of negative charge has been induced at the bottom electrode (Figure 6d). In this way a piezoelectric potential difference which has been produced between top and bottom electrode drives electron flows from one electrode to the top electrode through an external load without any external biasing. After withdrawal of compression, the dipoles immediately return back to their initial state by diminishing the piezoelectric potential sharply and an opposite electrical signal is produced due to opposite flow and accumulation of electrons via the external load.[4,14,50]

Performances and Proposed Working Mechanism of Self-Charged PPC. The high dielectric PCM3 film has been utilized as a storage unit for designing our highly efficient portable simplistic two electrode self-charged PPC. Our PPC has a solar energy to electrical energy converting part, i.e., MnO_2-MWCNT/PVP/H_3PO_4 film. The converted electrical

DOI: 10.1021/acssuschemeng.8b05080
ACS Sustainable Chem. Eng. 2019, 7, 4801−4813

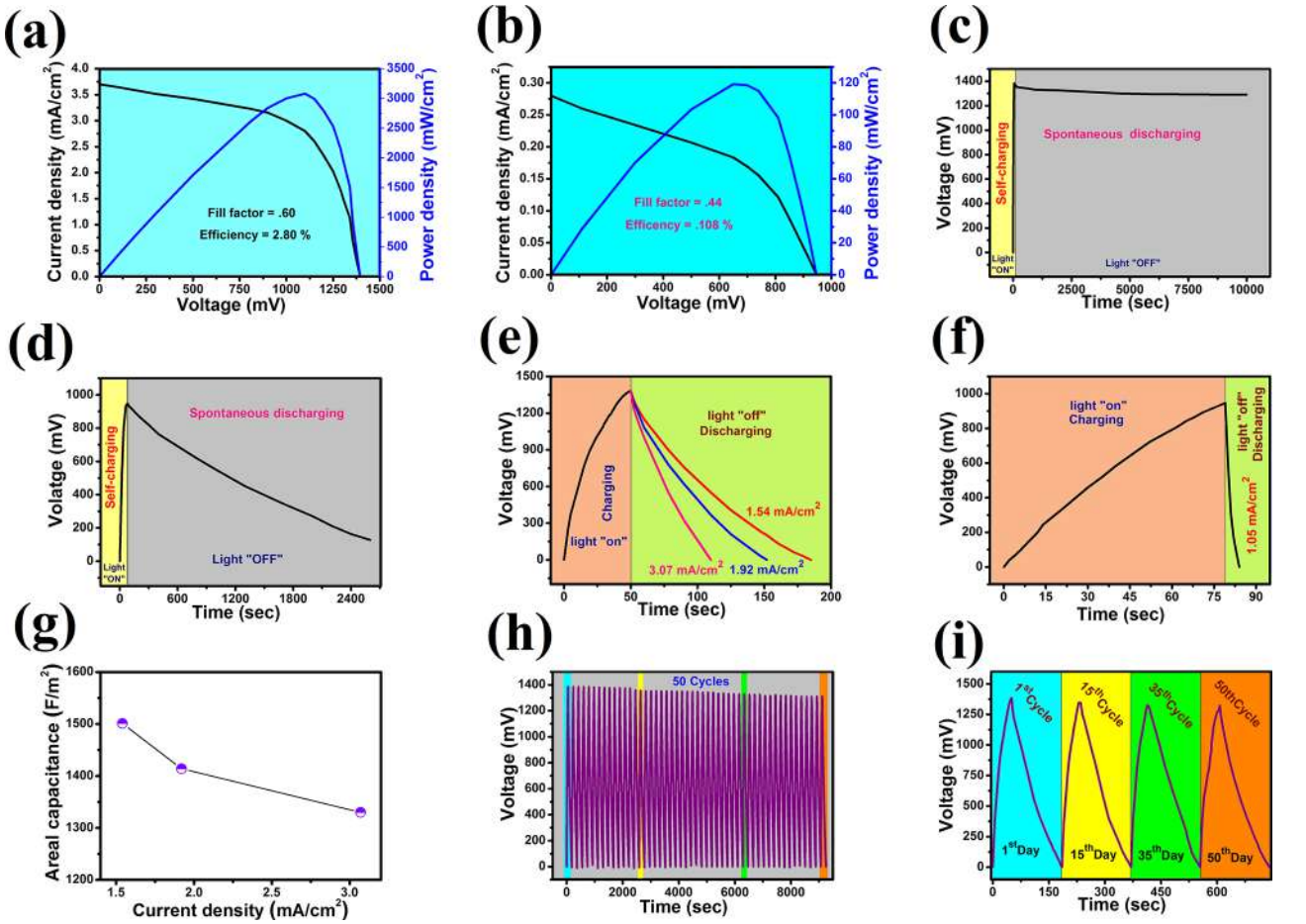

Figure 7. $J-V$ curves of PPC with (a) PCM3 thin film and (b) pure PVDF. (c, d) Self-charging and spontaneous discharging curves of PPC with PCM3 and pure PVDF film under light illumination and dark condition, respectively. (e, f) Self-charging and discharging curves with constant discharge current density. (g) Specific areal capacitance vs current density graph. (h, i) Self-charging and discharging performances over 50 cycles and magnified view of first, 15th, 35th, and 50th cycles of the PPC with PMC3 films.

energy is effectively stored into the PCM3 thin film in a single unit (Figure 1b).

Panels a and b Figure 7 represent the photocharacteristics, i.e., current density (J) vs voltage (V) and power (P) vs voltage (V) of our PPC containing pure PVDF and PCM3 films, respectively. The data are collected under illumination intensity (P_{in}) ~ 110 mW/cm^2 by a 40 W tungsten bulb having UV and IR blocking filters. Though highly efficient two electrode hybrid cell fabrication is more challenging as the presence of energy storage part reduces the energy conversion efficiency ($\eta_{conversion}$).Our PPC with PCM3 film shows good V_{oc} ~ 1.38 V, J_{sc} ~ 3.7 mA/cm^2, and fill factor (FF) ~ 0.60 with energy conversion efficiency ($\eta_{conversion}$) ~ 2.80%, which is many times greater than the PPC with pure PVDF shown in Table S5 (see the Supporting Information). The FF and $\eta_{conversion}$ are calculated by the following equations,

$$FF = (V_{mp}J_{mp})/(V_{oc}J_{sc}) \quad (4)$$

$$\eta_{conversion}/\% = \frac{(V_{oc}J_{sc}FF)}{P_{in}} \times 100 \quad (5)$$

Here,V_{mp} and J_{mp} are the voltage and current corresponding to maximum power point of PPC with pure PVDF or PCM3 film determined from the $J-V$ curve Figure 7a.

Panels c and d of Figure 7 denote the charging and spontaneous discharging phenomenon under light and dark condition of both of our PPCs, respectively. Our PPC with PCM3 film has been fully charged within a very short time ~50 s up to ~1.38 V under light illumination, whereas the PPC with pure PVDF film is charged up to ~0.947 V in ~79 s. The insertion of PCM3 film instead of pure PVDF into the PPC shows better output characteristics with significant charge storage stability. Under dark condition, the photovoltage of the PPC constructed with PCM3 film is almost constant (~1.38 V) (Figure 7c),over a long time, whereas the photovoltage of pure PVDF based PPC has discharged to 200 mV in a short time span due to internal recombination of charges (Figure 7d).

Excellent storage performance has been a characteristic of the PPC with PCM3 film under dark condition by the discharging of our PCM3 based PPC with three constant discharging current, 1.54, 1.92, and 3.07 mA/cm^2, respectively, shown in Figure 7e. The PPC with PCM3 film is fully discharged within 135, 102, and 60 s under the constant discharged current density 1.54, 1.92, and 3.07 mA/cm^2, respectively. The discharging process has also been performed for PPC with pure PVDF with constant discharge current density of 1.05 mA/cm^2 illustrated in Figure 7f. Furthermore, the accumulated charge density (Q_A), areal specific capacitance (C_A), energy density (E_{out}), and power density (P_A) of our

DOI: 10.1021/acssuschemeng.8b05080
ACS Sustainable Chem. Eng. 2019, 7, 4801−4813

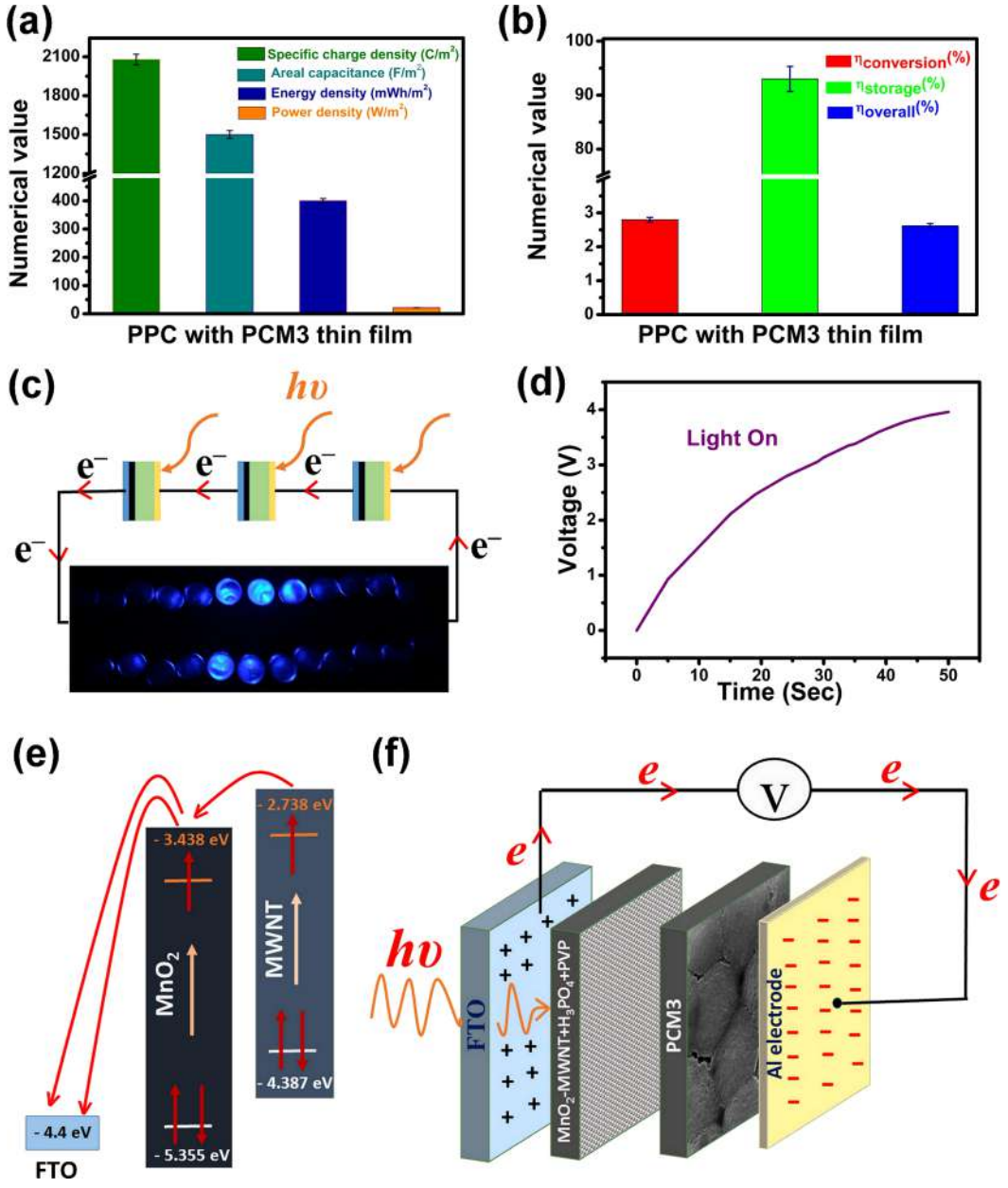

Figure 8. (a) Calculated areal capacitance, charge, and energy and power densities of our PMC3 based PCC from discharging graph. (b) Conversion, storage, and overall efficiencies of our device based on PCM3. (c) Schematic representation of glowing of LEDs by three serially connected PCM3 based PPC as power supplier. (d) $V-t$ charging graph of three serially connected PCM3 based PPC under visible light. (e) Energy diagram of the materials used as solar energy convertor (DFT calculation value). (f) Schematic presentation of photoelectrons creation and their storage in our PCM3 based PPC.

fabricated PPC with PCM3 and PPC with pure PVDF film have been evaluated from the discharge $V-t$ graph (Figure 7e,f, respectively) using the following equations:

$$Q_A = \left(\int I_{dis}\, dt_{dis}\right) \quad (6)$$

$$C_A = \left(\int I_{dis}\, dt_{dis}\right)/dV \quad (7)$$

$$E_{out} = 0.5 C_A V^2 \quad (8)$$

$$P_A = V I_{dis} \quad (9)$$

where I_A, dt_{dis}, dV, and V are the constant discharge current density, discharging time, discharging potential difference, and maximum voltage fully charged using light illumination, respectively.[4] Figure 7g represents the areal capacitance vs current density graph. Maximum specific areal capacitance has been obtained ~1501 F/m^2 for constant discharge current density ~ 1.54 mA/cm^2. The maximum value of specific charge density, energy density, and power density of PMC3 based PPC are calculated to be ~2079 C/m^2, 400.3 mWh/m^2, and 21.33 W/m^2, respectively, which results are much higher than the PPC with pure PVDF shown in Table S5 (see the Supporting Information).

The durability and recycling performances of our PCM3 based PPC has been performed for 50 charging−discharging cycles over 50 days (1 cycle/day) demonstrated in Figure 7h. Figure 7i represents the magnifying view for first, 15th, 35th,

DOI: 10.1021/acssuschemeng.8b05080
ACS Sustainable Chem. Eng. 2019, 7, 4801−4813

and 50th cycles of Figure 7h. After 50 days, the voltage generation ability of our PCM3 film based PPC decreases only ~5%. This decrease in photovoltage generation after 50 days (50 cycles) may be due to electron loss in external circuit, which leads to occurrence of irreversible redox reaction and formation of depletion layer at the junction between the solar part and the dielectric part. The storage efficiency ($\eta_{storage}$) and overall efficiency ($\eta_{overall}$) are calculated to be ~93% and 2.62% using eqs 10 and 11 (Figure 8a,b).The storage, conversion, and overall efficiencies of our PCM3 film based PPC are sufficiently higher than the efficiencies of PPC with pure PVDF film (seeTable S6 in the Supporting Information).

$$\eta_{storage}/\% = \frac{\eta_{overall}}{\eta_{conversion}} \times 100 \quad (10)$$

$$\eta_{overall}/\% = \frac{E_{out}}{E_{in}} \times 100 \quad (11)$$

$$E_{in} = P_{in}\, dt_{charg} \quad (12)$$

where E_{in} and dt_{charg} are the input energy density and charging time under light illumination, respectively.[51]

The output performances of our prototype PCM3 based PPC are much more promising than the other previously reported prototype photo-power unit or photo-supercapacitor with in situ storage systems (see comparison Table S6).[4,5,12,21−29,52,53]

Further, to verify the realistic utilization of our simplistic two electrode PCM3 film based PPC, commercially available LEDs are driven using three serially connected PPC with PCM3 film shown schematically in Figure 8c and Video S2 (see Supporting Information). First the three serially connected PPC is fully charged up to 3.95 V in just 50 s, shown in Figure 8d under light illumination. After the fully charge condition, our PCM3 based PPC is able to light up 24 blue LEDs (connected in parallel) continuously for 7 days, which proves superiority of our device for using as a power bank for portable electronic gadgets in our daily life.

Further, the working mechanism of our self-charged PPC may be explained considering the principle of a typical dye-sensitized solar cell and well established literature. Our PPC is not only able to harvest energy from light but also capable to store the photogenerated energy in the same unit. Thus, our proposed mechanism has been divided into two processes, i.e., creation of photoelectrons under light exposure and storage of the photogenerated electrons.[4,5,12,54,55]

In our PPC, MnO_2-MWCNT/PVP/H_3PO_4 film attached with the FTO is acting as electron−hole creator and the storage is mainly controlled by high dielectric PCM3 film. When the device is illuminated under visible light, the MWNT and MnO_2 are excited by absorbing the light ($h\nu$) and the electrons spring up to the LUMO state from the HOMO state (UV−visible spectra are shown in the Supporting Information (Figure S3). The excited electrons are moved to the FTO according to their energy configuration shown in Figure 8e. Thus, MWNT and MnO_2 are oxidized by losing the electrons.

$$MWNT + h\nu \rightarrow MWNT^* \rightarrow MWNT_{ox} + e^-$$

$$MnO_2 + h\nu \rightarrow MnO_2^* \rightarrow [MnO_2]_{ox} + e^-$$

Thereafter, the injected electrons on FTO are migrated to the counter electrode, i.e., Al, via connecting the external circuit and gathered at the junction between the Al and PCM3 as well as at the interfacial surfaces of CM and PVDF chains, which leads to formation of many microcapacitors in the high dielectric PCM3 film. At the same time, the photocreated holes in MWNT and MnO_2 are refilled by the donation of electrons through PVP/H_3PO_3 film which is acting as the solid electrolyte in our device. So, MWNT and MnO_2 are reduced to their original state and take part in the light absorbing and photoelectrons generation process once again.

$$PVP \leftrightarrow PVP^-$$

$$H_3PO_4 \leftrightarrow H^+ + H_2PO_4^{1-}$$

$$H_2PO_4^{1-} \leftrightarrow H^+ + HPO_4^{2-}$$

$$HPO_4^{2-} \leftrightarrow H^+ + PO_4^{3-}$$

$$MWNT_{ox} + PVP^- \rightarrow MWNT + PVP$$

$$MWNT_{ox} + H_3PO_4 \rightarrow [MWNT_{ox}][H_2PO_4^{1-} \text{ or } HPO_4^{2-}] + H^+$$

$$[MWNT_{ox}][H_2PO_4^{1-} \text{ or } HPO_4^{2-}] + H^+ + e \rightarrow MWNT_{red} + H_3PO_4$$

$$[MnO_2]_{ox} + PVP^- \rightarrow [MnO_2]_{red} + PVP$$

$$[MnO_2]_{ox} + H_3PO_4 \rightarrow [MnO_2]_{ox}[H_2PO_4^{1-} \text{ or } HPO_4^{2-}] + H^+$$

$$[MnO_2]_{ox}[H_2PO_4^{1-} \text{ or } HPO_4^{2-}] + H^+ + e \rightarrow [MnO_2]_{red} + H_3PO_4$$

Meanwhile, PVP and H_3PO_4 take part as ionic mediator and conductor of charge carriers. Continuous draining of electrons through PVP/H_3PO_4 film leads to net positive charges or holes accumulation at the interfaces of acting electrode and high dielectric PCM3 film.[56−61] Thus, an efficient potential difference has been originated between the two electrodes developing photovoltage in our PPC. When the open circuit voltage ~ 1.38 V, the oxidation and reduction processes of MWNT and MnO_2 are stopped and the current flow in the circuit becomes zero. The proposed mechanism of our self-charged PPC has been shown schematically in Figure 8f.

CONCLUSIONS

In summary, we have synthesized CTAB-MMT assisted electroactive ($F(\beta)$ ~ 91%) and high dielectric (~48 at 20 Hz) PVDF thin film via solution casting process and optimized the most appropriate thin film (PCM3) for fabricating two simplified, cost-effective, biocompatible, and lightweight two devices which can harvest electrical energy from mechanical energy and have solar energy converting ability with in situ storage function, respectively. Strong electrostatic interfacial interaction between the CM and the PVDF chains leads to electroactive β phase nucleation and large dielectric properties of the composite samples. Fabricated CMPENG exhibits good open circuit voltage (V_{oc}) ~ 41Vand short circuit current (I_{sc}) ~ 1.9 μA, which correspond to high power density ~ 50.72 mW/cm^{-3} under periodic finger impartation. Excellent mechanical to electrical power conversion efficiency ~ 60.2% in charging a capacitor has been achieved and 26 serially

DOI: 10.1021/acssuschemeng.8b05080
ACS Sustainable Chem. Eng. 2019, 7, 4801−4813

connected blue LEDs are driven by our CMPENG. Furthermore, the self-charged PCM3 based PPC shows superior recyclability and output performances with V_{oc} ~ 1.38 V and I_{sc} ~ 3.7 mA/cm^2 with remarkable storage and overall efficienc of ~93% and 2.62%, respectively. High specific areal capacitance ~ 1501 F/m^2 has been found with maximum power and energy density of ~21.33 W/m^2 and 400.3 mWh/m^2, respectively, for our PCM3 based PPC. Three combined PPC is also able to light up 24 blue LEDs continuously for 7 days after fully charged one time under light illumination. Thus, our two devices have the direct practical application possibilities in portable electronics as well as large scale energy dem\ands of our modern society.

■ ASSOCIATED CONTENT

Supporting Information

The Supporting Information is available free of charge on the ACS Publications website at DOI: 10.1021/acssuschemeng.8b05080.

Synthesis and characterization of CTAB-MMT, MWNT-MnO_2 composite; detailed calculations of force, piezoelectricity, and mechanical to electrical energy conversion efficiency (Table S1); comparisons of output characteristics of CMPENG (Tables S2, S3, and S4); self-charged PPC (Tables S5 and S6) (PDF)

Video S1 showing lighting of 26 blue LEDs under finger impartation on CMPENG connected in series (AVI)

Video S2 showing Lighting of 24 blue LEDs by self-charged PCM3 based PPC connected in parallel (AVI)

Video S3 showing measurement of output voltage generation by CMPENG under finger impartation (AVI)

Video S4 also showing measurement of output voltage generation by CMPENG under finger impartation (AVI)

■ AUTHOR INFORMATION

Corresponding Authors

*(P.T.) E-mail: pradipthakurju@gmail.com. Tel.: +919830366215.

*(S.D.) E-mail: sdasphysics@gmail.com. Tel.: +919433091337.

ORCID

Pradip Thakur: 0000-0003-3604-0736

Sukhen Das: 0000-0001-8372-3076

Notes

The authors declare no competing financial interest.

■ ACKNOWLEDGMENTS

We are grateful to the University Grant Commission (UGC), Government of India for financial assistance.

■ REFERENCES

(1) Chu, S.; Majumdar, A. Opportunities and challenges for a sustainable energy future. *Nature* **2012**, *488*, 294−303.

(2) Rosa, E. A.; Dietz, T. Human drivers of national greenhouse-gas emissions. *Nat. Clim. Change* **2012**, *2*, 581−586.

(3) Aubrecht, G. J.; Aubrecht, I.: *Energy: Physical, environmental, and social impact*, 3rd ed.; Pearson Prentice Hall: Upper Saddle River, NJ, USA, 2006.

(4) Thakur, P.; Kool, A.; Hoque, N. A.; Bagchi, B.; Khatun, F.; Biswas, P.; Brahma, D.; Roy, S.; Banerjee, S.; Das, S. Superior performances of in situ synthesized ZnO/PVDF thin film based self-poled piezoelectric nanogenerator and self-charged photo-power bank with high durability. *Nano Energy* **2018**, *44*, 456−467.

(5) Khatun, F.; Hoque, N. A.; Thakur, P.; Sepay, N.; Roy, S.; Bagchi, B.; Kool, A.; Das, S. 4′-Chlorochalcone-Assisted Electroactive Polyvinylidene Fluoride Film-Based Energy-Storage System Capable of Self-Charging Under Light. *Energy Technology* **2017**, *5*, 2205−2215.

(6) Wang, X.; Song, J.; Liu, J.; Wang, Z. L. Direct-current nanogenerator driven by ultrasonic waves. *Science* **2007**, *316*, 102−105.

(7) Chen, J.; Yang, J.; Guo, H.; Li, Z.; Zheng, L.; Su, Y.; Wen, Z.; Fan, X.; Wang, Z. L. Automatic mode transition enabled robust triboelectric nanogenerators. *ACS Nano* **2015**, *9*, 12334−12343.

(8) Ramadoss, A.; Saravanakumar, B.; Lee, S. W.; Kim, Y.-S.; Kim, S. J.; Wang, Z. L. Piezoelectric-driven self-charging supercapacitor power cell. *ACS Nano* **2015**, *9*, 4337−4345.

(9) Gu, L.; Cui, N.; Cheng, L.; Xu, Q.; Bai, S.; Yuan, M.; Wu, W.; Liu, J.; Zhao, Y.; Ma, F.; Qin, Y.; Wang, Z. L. Flexible fiber nanogenerator with 209 V output voltage directly powers a light-emitting diode. *Nano Lett.* **2013**, *13*, 91−94.

(10) Liu, J.; Cui, N.; Gu, L.; Chen, X.; Bai, S.; Zheng, Y.; Hu, C.; Qin, Y. A three-dimensional integrated nanogenerator for effectively harvesting sound energy from the environment. *Nanoscale* **2016**, *8*, 4938−4944.

(11) Yang, W.; Chen, J.; Zhu, G.; Yang, J.; Bai, P.; Su, Y.; Jing, Q.; Cao, X.; Wang, Z. L. Harvesting energy from the natural vibration of human walking. *ACS Nano* **2013**, *7*, 11317−11324.

(12) Roy, S.; Thakur, P.; Hoque, N. A.; Bagchi, B.; Sepay, N.; Khatun, F.; Kool, A.; Das, S. Electroactive and High Dielectric Folic Acid/PVDF Composite Film Rooted Simplistic Organic Photovoltaic Self-Charging Energy Storage Cell with Superior Energy Density and Storage Capability. *ACS Appl. Mater. Interfaces* **2017**, *9*, 24198−24209.

(13) Zhang, Q.; Dandeneau, C. S.; Zhou, X.; Cao, G. ZnO nanostructures for dye-sensitized solar cells. *Adv. Mater.* **2009**, *21*, 4087−4108.

(14) Hoque, N. A.; Thakur, P.; Roy, S.; Kool, A.; Bagchi, B.; Biswas, P.; Saikh, M. M.; Khatun, F.; Das, S.; Ray, P. P. Er3+/Fe3+ Stimulated Electroactive, Visible Light Emitting, and High Dielectric Flexible PVDF Film Based Piezoelectric Nanogenerators: A Simple and Superior Self-Powered Energy Harvester with Remarkable Power Density. *ACS Appl. Mater. Interfaces* **2017**, *9*, 23048−23059.

(15) Wu, J. M.; Chen, K.-H.; Zhang, Y.; Wang, Z. L. A self-powered piezotronic strain sensor based on single ZnSnO3 microbelts. *RSC Adv.* **2013**, *3*, 25184−25189.

(16) Park, K. I.; Son, J. H.; Hwang, G. T.; Jeong, C. K.; Ryu, J.; Koo, M.; Choi, I.; Lee, S. H.; Byun, M.; Wang, Z. L.; Lee, K. J. Highly-efficient, flexible piezoelectric PZT thin film nanogenerator on plastic substrates. *Adv. Mater.* **2014**, *26*, 2514−2520.

(17) Lin, Z.-H.; Yang, Y.; Wu, J. M.; Liu, Y.; Zhang, F.; Wang, Z. L. BaTiO3 nanotubes-based flexible and transparent nanogenerators. *J. Phys. Chem. Lett.* **2012**, *3*, 3599−3604.

(18) Xu, S.; Yeh, Y.-w.; Poirier, G.; McAlpine, M. C.; Register, R. A.; Yao, N. Flexible piezoelectric PMN−PT nanowire-based nanocomposite and device. *Nano Lett.* **2013**, *13*, 2393−2398.

(19) Kang, H. B.; Chang, J.; Koh, K.; Lin, L.; Cho, Y. S. High quality Mn-doped (Na, K) NbO3 nanofibers for flexible piezoelectric nanogenerators. *ACS Appl. Mater. Interfaces* **2014**, *6*, 10576−10582.

(20) Chang, C.; Tran, V. H.; Wang, J.; Fuh, Y.-K.; Lin, L. Direct-write piezoelectric polymeric nanogenerator with high energy conversion efficiency. *Nano Lett.* **2010**, *10*, 726−731.

(21) Wee, G.; Salim, T.; Lam, Y. M.; Mhaisalkar, S. G.; Srinivasan, M. Printable photo-supercapacitor using single-walled carbon nanotubes. *Energy Environ. Sci.* **2011**, *4*, 413−416.

(22) Chien, C. T.; Hiralal, P.; Wang, D. Y.; Huang, I. S.; Chen, C. C.; Chen, C. W.; Amaratunga, G. A. Graphene-Based Integrated Photovoltaic Energy Harvesting/Storage Device. *Small* **2015**, *11*, 2929−2937.

DOI: 10.1021/acssuschemeng.8b05080
ACS Sustainable Chem. Eng. 2019, 7, 4801−4813

(23) Chen, T.; Qiu, L.; Yang, Z.; Cai, Z.; Ren, J.; Li, H.; Lin, H.; Sun, X.; Peng, H. An integrated "energy wire" for both photoelectric conversion and energy storage. *Angew. Chem., Int. Ed.* **2012**, *51*, 11977−11980.
(24) Yan, J. M.; Wang, Z. L.; Gu, L.; Li, S. J.; Wang, H. L.; Zheng, W. T.; Jiang, Q. AuPd−MnOx/MOF−graphene: An efficient catalyst for hydrogen production from formic acid at room temperature. *Adv. Energy Mater.* **2015**, *5*, 1500107.
(25) Chen, X.; Wu, Z.; Xu, S.; Wang, L.; Huang, R.; Han, Y.; Ye, W.; Xiong, W.; Han, T.; Long, G.; Wang, Y.; He, Y.; Cai, Y.; Sheng, P.; Wang, N. Probing the electron states and metal-insulator transition mechanisms in molybdenum disulphide vertical heterostructures. *Nat. Commun.* **2015**, *6*, 6088.
(26) Zhou, F.; Ren, Z.; Zhao, Y.; Shen, X.; Wang, A.; Li, Y. Y.; Surya, C.; Chai, Y. Perovskite photovoltachromic supercapacitor with all-transparent electrodes. *ACS Nano* **2016**, *10*, 5900−5908.
(27) Murakami, T. N.; Kawashima, N.; Miyasaka, T. A high-voltage dye-sensitized photocapacitor of a three-electrode system. *Chem. Commun.* **2005**, 3346−3348.
(28) Zhang, M.; Zhou, Q.; Chen, J.; Yu, X.; Huang, L.; Li, Y.; Li, C.; Shi, G. An ultrahigh-rate electrochemical capacitor based on solution-processed highly conductive PEDOT: PSS films for AC line-filtering. *Energy Environ. Sci.* **2016**, *9*, 2005−2010.
(29) Zhang, X.; Huang, X.; Li, C.; Jiang, H. Dye-sensitized solar cell with energy storage function through PVDF/ZnO nanocomposite counter electrode. *Adv. Mater.* **2013**, *25*, 4093−4096.
(30) Martins, P.; Lopes, A.; Lanceros-Mendez, S. Electroactive phases of poly (vinylidene fluoride): determination, processing and applications. *Prog. Polym. Sci.* **2014**, *39*, 683−706.
(31) Thakur, P.; Kool, A.; Bagchi, B.; Hoque, N. A.; Das, S.; Nandy, P. In situ synthesis of Ni (OH) 2 nanobelt modified electroactive poly (vinylidene fluoride) thin films: remarkable improvement in dielectric properties. *Phys. Chem. Chem. Phys.* **2015**, *17*, 13082−13091.
(32) Das-Gupta, D.; Doughty, K. Corona charging and the piezoelectric effect in polyvinylidene fluoride. *J. Appl. Phys.* **1978**, *49*, 4601−4603.
(33) Bao, S.; Liang, G.; Tjong, S. C. Effect of mechanical stretching on electrical conductivity and positive temperature coefficient characteristics of poly (vinylidene fluoride)/carbon nanofiber composites prepared by non-solvent precipitation. *Carbon* **2011**, *49*, 1758−1768.
(34) Mandal, D.; Henkel, K.; Schmeißer, D. The electroactive β-phase formation in poly (vinylidene fluoride) by gold nanoparticles doping. *Mater. Lett.* **2012**, *73*, 123−125.
(35) Thakur, P.; Kool, A.; Bagchi, B.; Das, S.; Nandy, P. Effect of in situ synthesized Fe 2 O 3 and Co 3 O 4 nanoparticles on electroactive β phase crystallization and dielectric properties of poly (vinylidene fluoride) thin films. *Phys. Chem. Chem. Phys.* **2015**, *17*, 1368−1378.
(36) Thakur, P.; Kool, A.; Hoque, N. A.; Bagchi, B.; Roy, S.; Sepay, N.; Das, S.; Nandy, P. Improving the thermal stability, electroactive β phase crystallization and dielectric constant of NiO nanoparticle/C−NiO nanocomposite embedded flexible poly (vinylidene fluoride) thin films. *RSC Adv.* **2016**, *6*, 26288−26299.
(37) Wu, W.; Huang, X.; Li, S.; Jiang, P.; Toshikatsu, T. Novel three-dimensional zinc oxide superstructures for high dielectric constant polymer composites capable of withstanding high electric field. *J. Phys. Chem. C* **2012**, *116*, 24887−24895.
(38) Mendes, S. F.; Costa, C. M.; Caparrós, C.; Sencadas, V.; Lanceros-Méndez, S. Effect of filler size and concentration on the structure and properties of poly (vinylidene fluoride)/BaTiO3 nanocomposites. *J. Mater. Sci.* **2012**, *47*, 1378−1388.
(39) Thakur, P.; Kool, A.; Bagchi, B.; Hoque, N. A.; Das, S.; Nandy, P. The role of cerium (iii)/yttrium (iii) nitrate hexahydrate salts on electroactive β phase nucleation and dielectric properties of poly (vinylidene fluoride) thin films. *RSC Adv.* **2015**, *5*, 28487−28496.
(40) Li, Y.-J.; Xu, M.; Feng, J.-Q.; Dang, Z.-M. Dielectric behavior of a metal-polymer composite with low percolation threshold. *Appl. Phys. Lett.* **2006**, *89*, 072902.
(41) Benz, M.; Euler, W. B.; Gregory, O. J. The role of solution phase water on the deposition of thin films of poly (vinylidene fluoride). *Macromolecules* **2002**, *35*, 2682−2688.
(42) Yuan, J.-K.; Yao, S.-H.; Dang, Z.-M.; Sylvestre, A.; Genestoux, M.; Bai, J. Giant dielectric permittivity nanocomposites: Realizing true potential of pristine carbon nanotubes in polyvinylidene fluoride matrix through an enhanced interfacial interaction. *J. Phys. Chem. C* **2011**, *115*, 5515−5521.
(43) Thakur, P.; Kool, A.; Bagchi, B.; Das, S.; Nandy, P. Enhancement of β phase crystallization and dielectric behavior of kaolinite/halloysite modified poly (vinylidene fluoride) thin films. *Appl. Clay Sci.* **2014**, *99*, 149−159.
(44) Peng, G.; Wang, L.; Li, F.; Luo, P. Structure and dielectric performance of poly (vinylidene fluoride)/organically modified montmorillonites nanocomposites. *J. Elastomers Plast.* **2016**, *48*, 251−265.
(45) Thomas, E.; Parvathy, C.; Balachandran, N.; Bhuvaneswari, S.; Vijayalakshmi, K. P.; George, B. K. PVDF-ionic liquid modified clay nanocomposites: Phase changes and shish-kebab structure. *Polymer* **2017**, *115*, 70−76.
(46) Wang, P.; Ma, J.; Wang, Z.; Shi, F.; Liu, Q. Enhanced separation performance of PVDF/PVP-g-MMT nanocomposite ultrafiltration membrane based on the NVP-grafted polymerization modification of montmorillonite (MMT). *Langmuir* **2012**, *28*, 4776−4786.
(47) Roy, S.; Thakur, P.; Hoque, N. A.; Bagchi, B.; Das, S. Enhanced electroactive β-phase nucleation and dielectric properties of PVdF-HFP thin films influenced by montmorillonite and Ni (OH) 2 nanoparticle modified montmorillonite. *RSC Adv.* **2016**, *6*, 21881−21894.
(48) Dakin, T. Conduction and polarization mechanisms and trends in dielectric. *IEEE Electrical Insulation Magazine* **2006**, *22*, 11−28.
(49) Mandal, D.; Henkel, K.; Schmeißer, D. Improved performance of a polymer nanogenerator based on silver nanoparticles doped electrospun P (VDF−HFP) nanofibers. *Phys. Chem. Chem. Phys.* **2014**, *16*, 10403−10407.
(50) Karan, S. K.; Bera, R.; Paria, S.; Das, A. K.; Maiti, S.; Maitra, A.; Khatua, B. B. An Approach to Design Highly Durable Piezoelectric Nanogenerator Based on Self-Poled PVDF/AlO-rGO Flexible Nanocomposite with High Power Density and Energy Conversion Efficiency. *Adv. Energy Mater.* **2016**, *6*, 1601016.
(51) Liu, Z.; Zhong, Y.; Sun, B.; Liu, X.; Han, J.; Shi, T.; Tang, Z.; Liao, G. Novel Integration of Perovskite Solar Cell and Supercapacitor Based on Carbon Electrode for Hybridizing Energy Conversion and Storage. *ACS Appl. Mater. Interfaces* **2017**, *9*, 22361−22368.
(52) Xu, X.; Li, S.; Zhang, H.; Shen, Y.; Zakeeruddin, S. M.; Graetzel, M.; Cheng, Y.-B.; Wang, M. A power pack based on organometallic perovskite solar cell and supercapacitor. *ACS Nano* **2015**, *9*, 1782−1787.
(53) Shi, C.; Dong, H.; Zhu, R.; Li, H.; Sun, Y.; Xu, D.; Zhao, Q.; Yu, D. An "all-in-one" mesh-typed integrated energy unit for both photoelectric conversion and energy storage in uniform electrochemical system. *Nano Energy* **2015**, *13*, 670−678.
(54) Cohn, A. P.; Erwin, W. R.; Share, K.; Oakes, L.; Westover, A. S.; Carter, R. E.; Bardhan, R.; Pint, C. L. All silicon electrode photocapacitor for integrated energy storage and conversion. *Nano Lett.* **2015**, *15*, 2727−2731.
(55) Skunik-Nuckowska, M.; Grzejszczyk, K.; Kulesza, P. J.; Yang, L.; Vlachopoulos, N.; Häggman, L.; Johansson, E.; Hagfeldt, A. Integration of solid-state dye-sensitized solar cell with metal oxide charge storage material into photoelectrochemical capacitor. *J. Power Sources* **2013**, *234*, 91−99.
(56) Khatun, F.; Thakur, P.; Hoque, N. A.; Kool, A.; Roy, S.; Biswas, P.; Bagchi, B.; Das, S. In situ synthesized SrF2/polyvinylidene fluoride nanocomposite film based photo-power cell with imperious performance and stability. *Electrochim. Acta* **2018**, *282*, 194−204.
(57) Khatun, F.; Thakur, P.; Amin Hoque, N.; Kool, A.; Roy, S.; Biswas, P.; Bagchi, B.; Das, S. In situ synthesized electroactive and

DOI: 10.1021/acssuschemeng.8b05080
ACS Sustainable Chem. Eng. 2019, 7, 4801−4813

large dielectric BaF2/PVDF nanocomposite film for superior and highly durable self-charged hybrid photo-power cell. *Energy Convers. Manage.* **2018**, *171*, 1083−1092.
(58) Gao, H.; Lian, K. Proton-conducting polymer electrolytes and their applications in solid supercapacitors: a review. *RSC Adv.* **2014**, *4*, 33091−33113.
(59) Greenwood, N. N.; Thompson, A. The Mechanism of Electrical Conduction in Fused Phosphoric and Trideuterophosphoric Acids. *J. Chem. Soc.* **1959**, *0*, 3485−3492.
(60) Vega-Garita, V.; Ramirez-Elizondo, L.; Narayan, N.; Bauer, P. Integrating a photovoltaic storage system in one device: A critical review. *Prog. Photovoltaics* **2018**, 1−25.
(61) Selvam, S.; Balamuralitharan, B.; Karthick, S. N.; Savariraj, A. D.; Hemalatha, K. V.; Kim, S.-K.; Kim, H.-J. Novel high-temperature supercapacitor combined dye sensitized solar cell from a sulfated *β*-cyclodextrin/PVP/MnCO3 composite. *J. Mater. Chem. A* **2015**, *3* (19), 10225−10232.

DOI: 10.1021/acssuschemeng.8b05080
ACS Sustainable Chem. Eng. 2019, 7, 4801−4813